



Validation of an aeroelastic model of Vestas V39

Larsen, Gunner Chr.; Vølund, P.

Publication date:
1998

Document Version
Publisher's PDF, also known as Version of record

[Link back to DTU Orbit](#)

Citation (APA):
Larsen, G. C., & Vølund, P. (1998). *Validation of an aeroelastic model of Vestas V39*. Denmark. Forskningscenter Risøe. Risøe-R No. 1051(EN)

General rights

Copyright and moral rights for the publications made accessible in the public portal are retained by the authors and/or other copyright owners and it is a condition of accessing publications that users recognise and abide by the legal requirements associated with these rights.

- Users may download and print one copy of any publication from the public portal for the purpose of private study or research.
- You may not further distribute the material or use it for any profit-making activity or commercial gain
- You may freely distribute the URL identifying the publication in the public portal

If you believe that this document breaches copyright please contact us providing details, and we will remove access to the work immediately and investigate your claim.

Validation of an Aeroelastic Model of Vestas V39

MASTER

Gunner Chr. Larsen and Per Vølund

RECEIVED

AUG 10 1998

OSTI

DISTRIBUTION OF THIS DOCUMENT IS UNLIMITED
FOREIGN SALES PROHIBITED

NT

DISCLAIMER

Portions of this document may be illegible electronic image products. Images are produced from the best available original document.

Validation of an Aeroelastic Model of Vestas V39

Gunner Chr. Larsen and Per Vølund

Abstract

An aeroelastic model of the pitch controlled wind turbine Vestas V39 is validated by comparison of predictions and measurements. The aeroelastic code used is HawC, which has been developed at Risø, and the turbulence model is the Mann model. The measurements used for the validation were carried out in complex terrain at the Sky River wind farm in California. The comparisons are carried out on a statistical basis as well as on power spectra level, and show a fully satisfactory agreement between predictions and measurements.

The model has subsequently been used for investigation of load sensitivity to wind and turbulence parameters for a complex terrain in the project COMTERID.

The work reported makes part of the project "Investigation of Design Aspects & Design Options for Wind Turbines Operating in Complex Terrain Environments" (COMTERID), which is co-funded through JOULEIII under contract no. JOR3-CT95-0033.

ISBN 87-550-2391-6
ISSN 0106-2840

Information Service Department, Risø, 1998

Contents

1. INTRODUCTION	5
2. AEROELASTIC MODEL	6
2.1 HawC	6
2.2 Vestas V39 model	9
3. CHARACTERISATION OF SITE AND LOAD CASES	10
3.1 Site	10
3.2 Load cases	14
4. RESULTS	16
4.1 Statistics of measurements and predictions	16
4.2 Power spectra of measurements and predictions	22
5. CONCLUSION	28
6. REFERENCES	29

1. Introduction

In this report an aeroelastic model of the Vestas V39 turbine is validated. The turbine is a pitch controlled, three bladed, upwind and constant speed machine with an active yaw mechanism. It has a rotor diameter of 39m, a hub height of 40m, and a rated power equal to 500kW. A detailed description of the turbine is found in (Petersen, 1994).

Basically, the present aeroelastic model is identical to the model used for the Sky River investigations reported in (Thomsen, 1996). However, some fine tuning associated with structural damping of blades, shaft and tower has been performed.

As the model already is validated to some extent (Thomsen, 1996), it has been decided to base the present fine tuning and validation on only two load cases representing a medium wind speed situation and a high wind speed situation, respectively. The involved measurements originate from a complex terrain site at Sky River in California. The validation is performed by comparing statistical parameters as well as power spectra of selected structural loads.

The report is structured as follows. Chapter 2 contains a description of the aeroelastic code. In Chapter 3 a brief characterisation of the terrain and the selected load cases are outlined. Then follows in Chapter 4 a comparison of simulated and measured loads for the relevant load cases. Finally, the conclusion of the validation is presented in Chapter 5.

2. Aeroelastic model

In this chapter the aeroelastic model of the Vestas V39 turbine is described. The model is based on the "Horizontal axis wind turbine simulation Code", HawC, which is described in detail in (Thirstrup Petersen, 1990). The main features of the code is briefly recapitulated below.

2.1 HawC

HawC is basically a finite element model developed as a special purpose wind turbine model. The rotating substructures, i. e. nacelle and rotor, makes it special compared to general purpose finite element programs. Usually these do not offer a satisfactory modelling of rotating substructures.

The structural model is based on 2-node prismatic beam elements with 6 degrees of freedom at each node, corresponding to 3 translations and 3 rotations. The interpolation functions are polynomials of 3rd order, representing the solutions to the equilibrium equations for the element. The wind turbine structure is subdivided into 3 substructures: tower, shaft/nacelle and rotor. The shaft/nacelle and the rotor are described as rotating substructures, coupled to each other and to the tower. An example of a typical division of the wind turbine in finite elements is shown in Figure 2.1-1. A more detailed picture of the division in elements on the blade is shown in Figure 2.1-2.

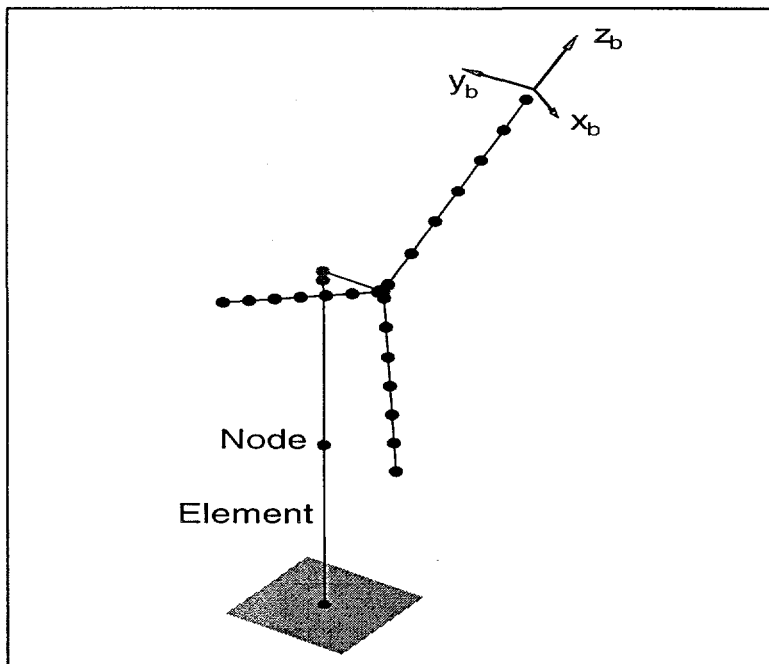


Figure 2.1-1 Finite element model of wind turbine.

Real blades are tapered and twisted, whereas the available structural finite elements are prismatic, and thus the model is an approximation. In Figure 2.1-2, a section of the blade is shown in the figure part A and the corresponding model in figure part B, where 2 elements are chosen. The (x_b, y_b, z_b) -coordinate system is a common blade system, with the z_b -axis pointing radially outwards. Each element in B is described in a local element coordinate system - for element no. 'i' the system is denoted x_{pi}, y_{pi}, z_{pi} - with the x_{pi} and y_{pi} axes coinciding with the principal bending axes, and the z_{pi} axis coinciding with the elastic axis. The orientation of the local x_{pi} and y_{pi} axis is usually chosen as the orientation of the principal axes at the midpoint of the real element, resulting in an approximation to the

structural blade twist. In the figure the z_{pi} axes are assumed to coincide with the common z_p axis, which need not be the case. In addition to principal bending axes and elastic axis the structural element is described by cross sectional centres for mass and shear.

The aerodynamic geometry is not influenced by the structural element division.

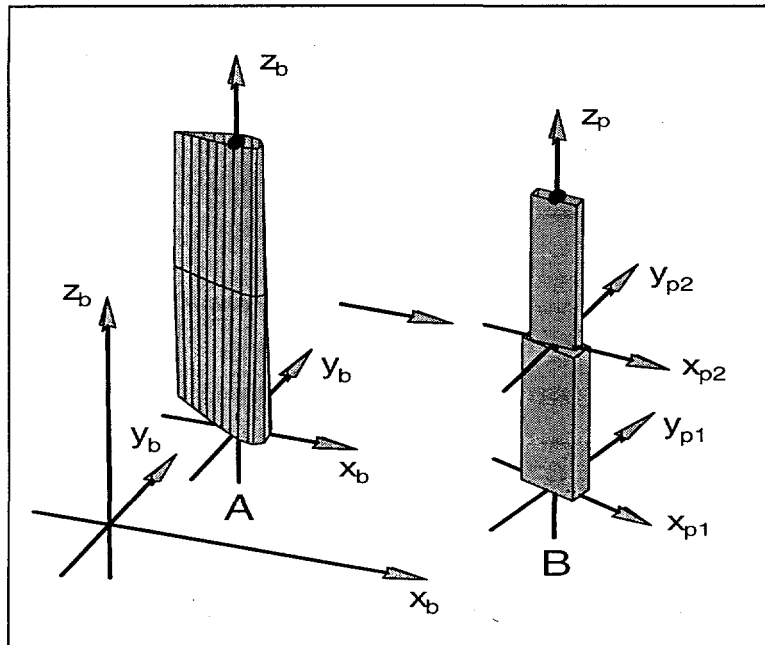


Figure 2.1-2 Finite elements of blade.

The elastic deformations, including rotations, as well as the bearing restrained rotations at the coupling nodes are taken into account in the expressions for the inertia loads on the substructures. Distributed loads on the elements (inertia, aerodynamic and gravity) are consistently transformed to the nodes. This results in a complete coupled dynamic model for the response of the wind turbine to external loading described by a set of discrete, non-linear, ordinary differential equations with time varying coefficients, comprising the equations of motion, which arranged as a matrix equation has the general form

$$[M]\{\ddot{x}\} + [C]\{\dot{x}\} + [K]\{x\} = \{F\}$$

where

[M] is the mass matrix, which is time varying due to bearing restrained, time dependent changes of geometry,

[C] is the time varying combined structural damping and Coriolis/gyroscopic matrix,

[K] is the time varying combined structural, geometrical and inertia stiffness matrix,

{F} is the force vector composed of terms originating from aerodynamic loads, gravity loads and inertia loads, which have not been resolved in terms which could be included in the left hand side expressions

{x} is the vector of translations and rotations

The flexible elements of the drive train are modelled as shaft elements with mass, structural damping and stiffness. The generator is modelled as a separate rotational degree of freedom with mass moment of inertia and a torque corresponding to the actual generator characteristic, which can be explicitly prescribed in a subroutine. An asynchronous generator is used for the turbine involved in the present work. Its characteristic is equivalent to a damping term, which can be adequately derived from the slip and the nominal torque. All properties of high speed shaft elements and generator are transformed to the low speed shaft side of the gear box.

The model offers the possibility of calculating the coupled mode shapes and natural frequencies for the rotating turbine as well as for the turbine at stand still. The facility is frequently used to compare the dynamic properties of the modelled turbine with the properties of the real one, for which the fundamental frequencies have often been determined with good accuracy. This check is further a guideline for choosing an appropriate number of elements in the finite element model.

The structural damping is modelled as proportional damping, i.e. a linear combination of the mass and the stiffness matrices. Choice of its actual magnitude is based on experience. Its inclusion is of particular importance when considering dynamic activity at, or close to, the natural frequencies.

Aerodynamic load and wind field

The aerodynamic loads are derived by use of a quasi-steady theory, based on combined blade element and momentum theory. The calculation of induced velocity can be based on either the frozen wake or the equilibrium wake approximation. No model for dynamic inflow has been included in the code so far.

The model for aerodynamic load calculation is fully aeroelastic, in that the influence of the elastic deformations on the aerodynamic force is taken into account.

The free wind vector is composed of a deterministic contribution including wind shear and tower interference, and a stochastic component, which can be generated according to either the Mann- or the Sandia method for time simulation of turbulence.

The wind shear is described by either a log- or a power-law, or alternatively the shear field might be predefined through definition as a vector field on an planar grid perpendicular to the mean wind direction at hub height, which is read from a file.

The tower interference is taken into account by use of a potential flow model. An example of the longitudinal v_y component of an arbitrary predefined shear field influenced by the tower shadow is shown in Figure 2.1-3.

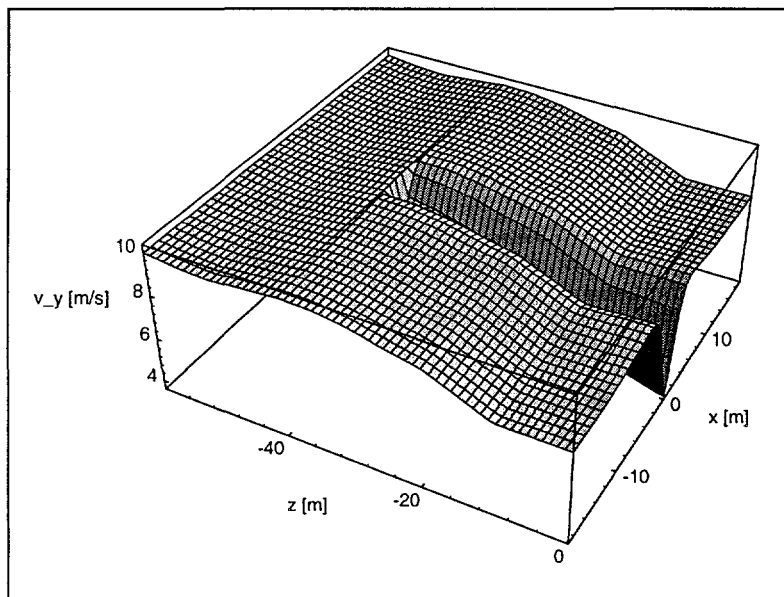


Figure 2.1-3 Predefined shear (longitudinal component) influenced by tower. $z=0\text{m}$ corresponds to ground level.

Mann turbulence model

The Mann turbulence simulation method is used in the present simulations. It is based on a model of a spectral tensor for the atmospheric surface layer turbulence at high wind speeds, corresponding to neutral stratification. The model is described in (Mann, 1994). The model assumes that the turbulence is homogeneous in space but non-isotropic and includes the influence of shear. The method generates a full three-dimensional turbulence field with all three components.

The turbulence is generated in a rectangular box with quadratic cross section corresponding to the plane perpendicular to the mean wind direction at points placed on a rectangular grid. In the present application of the method there are 16*16 points available on a quadratic grid on a cross section and 4096 points in the along wind direction. The grid points are equally spaced in all directions. The generated turbulence is scaled and stored on disk. The only parameters needed for scaling to actual conditions are hub height, mean wind speed and terrain roughness length.

In order to obtain a reasonable turbulence for complex terrain from the homogeneous Mann field, a facility has been added to the aeroelastic code, which offers the possibility of scaling the turbulence intensity individually for the 3 directions. This will of course add some distortion to the spatial structure of the turbulence, which may not be in agreement with the actual measured field.

Solution of equations of motion

Having established the full system of equations of motions based on the sub-models outlined above, this is solved, at each time step, by use of the Newmark implicit time integration scheme. Iterations are performed at each time step in order to obtain equilibrium within certain prescribed limits.

2.2 Vestas V39 model

In order to adjust the options offered in HawC to the present modelling of the Vestas V39 turbine, it was (rather arbitrarily) chosen to express the structural damping term as proportional to the stiffness only. For each main component (blade(s), main shaft, and tower) three proportionally constants were adjusted - one for each deflection type (2 bending and one torsion).

It was moreover chosen to base all the present results on the frozen wake approximation and thus exclude the equilibrium wake consideration.

The pitch control in the model is equivalent to the control on the real turbine; i.e. the blade is pitched both structurally and aerodynamically, controlled by an algorithm identical to the one applied on the real turbine. Even though the Vestas V39 turbine is a pitch controlled turbine, a simple time-lag stall model is included in the present aerodynamic modelling in order to deal with possible large angles of flow incidence on the inner part of the blades.

3. Characterisation of site and load cases

The measurements involved in the validation originate from the Sky River wind farm in California. Two different load cases are selected representing different mean wind and turbulence intensity regimes.

3.1 Site

The Sky River wind farm is situated in a complex mountainous terrain with only a few fences and trees. The wind regime is primarily thermally driven causing two very distinct prevailing wind directions. Combined with the topography of the wind farm, this means that the instrumented turbine hardly ever operated under wake conditions during the measuring campaign. Consequently, the instrumented turbine can be considered as a stand alone turbine.

The wind field observed at Sky River differ from a traditional flat terrain wind field on different respects that affect the turbine loading. First of all, the density of the air is reduced due to the altitude, which affect both the periodic deterministic- and the turbulence driven aerodynamic forces. In the present situation the density of the air is reduced from 1.225kg/m^3 to 1.04kg/m^3 .

In addition to the effect arising from the modification of the air density, the deterministic aerodynamic forces are adjusted due to the actual terrain slope and the particular shear field associated with the site. The terrain slope causes the mean wind direction to form an angle with the horizontal plane. The magnitude of the angle depends on the level above ground. However, in the present situation only the angles associated with the region represented by the rotor plane is of relevance. The situation is illustrated in Figures 3.1-1 and 3.1-2 where the mean wind slope, with the horizontal plane, has been plotted as function of the mean wind speed for a large number of 10 min. averages based on sonic measurements performed at 19.3m and 42.7m above terrain, respectively.

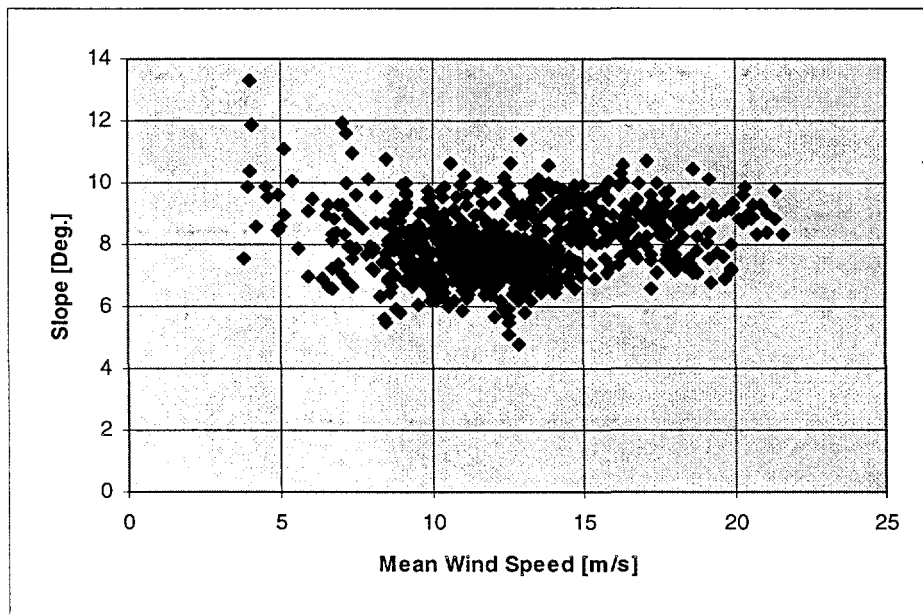


Figure 3.1-1 Slope of mean wind direction based on sonic measurements at level 19.3m.

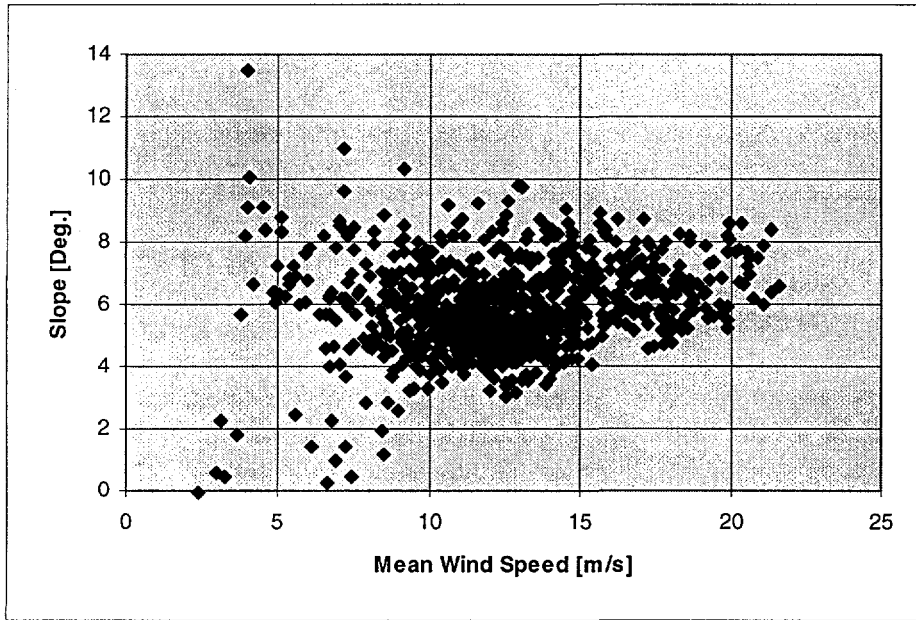


Figure 3.1-2 Slope of mean wind direction based on sonic measurements at level 42.7m.

The mean wind shear in the present situation differ from the traditional log- or power-law description due to speed up effects caused by the topography of the landscape. The particular shape of the shear field in the rotor plane region is dealt with in section 3.2.

The stochastic part of the aerodynamic forces, driven by the turbulence, is traditionally determined based on specifications of the turbulence intensities, the turbulence length scales, and the coherences between arbitrary turbulence components. For the Sky River site, measured turbulence intensities are presented in the Figures 3.1-3, 3.1-4, 3.1-5, 3.1-6 and 3.1-7.

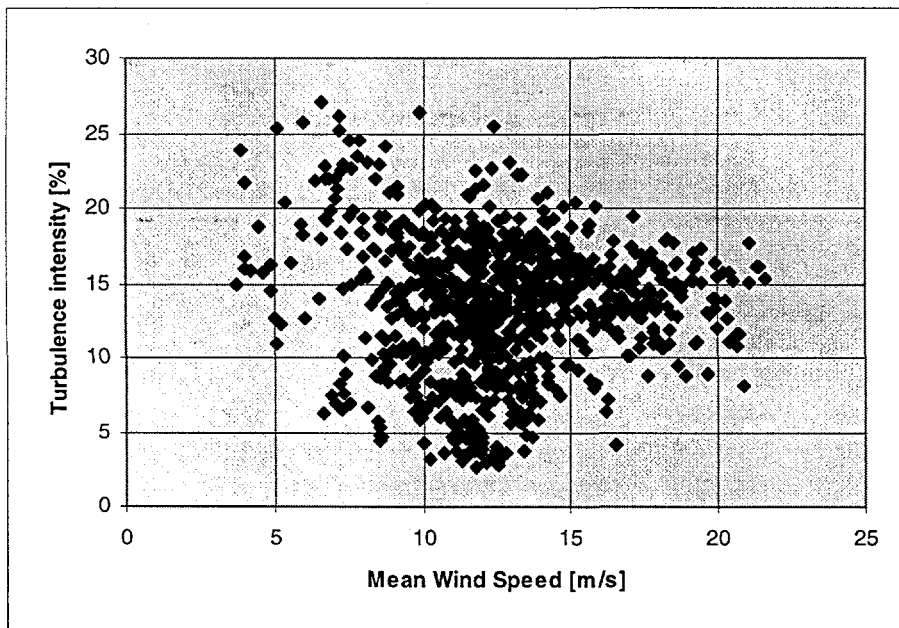


Figure 3.1-3 Turbulence intensity of the horizontal wind component as function of mean wind speed.

The turbulence intensity presented in Figure 3.1-3 is based on cup anemometer measurements at level 42.7 m, and it is seen to exhibit considerable variations. As the site is characterised by only two prevailing wind directions, it is not likely that the variations should be caused by varying upstream terrain conditions. The phenomenon is believed to be caused by huge variations in the stability conditions which is supported by the fact that the turbulence intensity variations tends to diminish with increasing wind speed where the mechanical turbulence contribution tends gradually to dominate the temperature driven contribution at higher wind speeds, thus approaching neutral conditions and less variations in stability conditions.

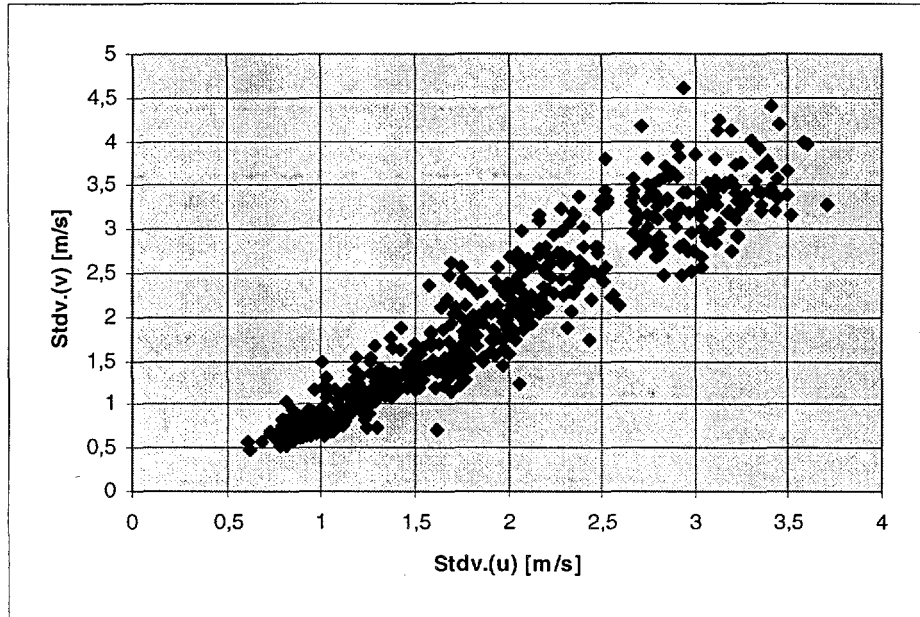


Figure 3.1-4 Standard deviation of the v turbulence component as function of standard deviation of the u turbulence component at level 19.3 m.

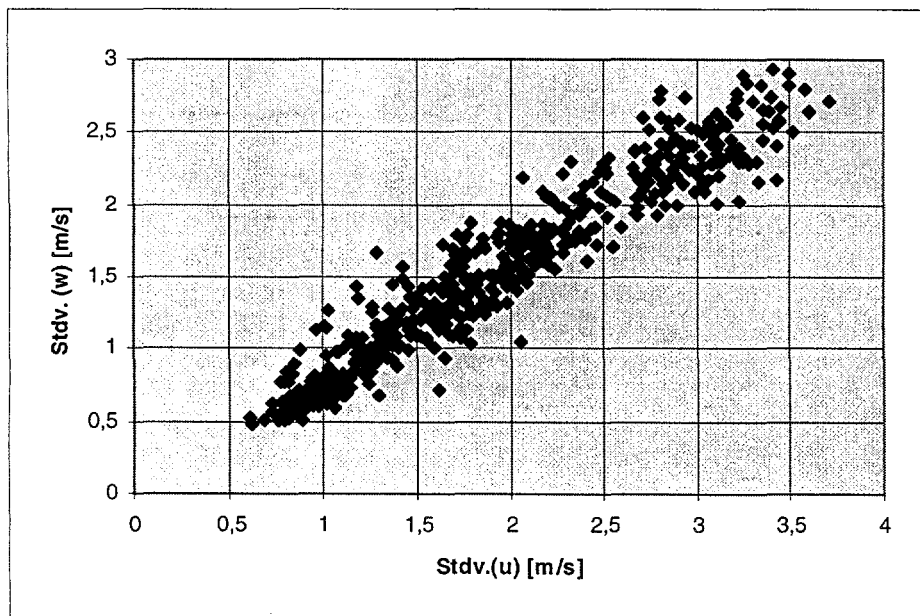


Figure 3.1-5 Standard deviation of the v turbulence component as function of standard deviation of the u turbulence component at level 19.3 m.

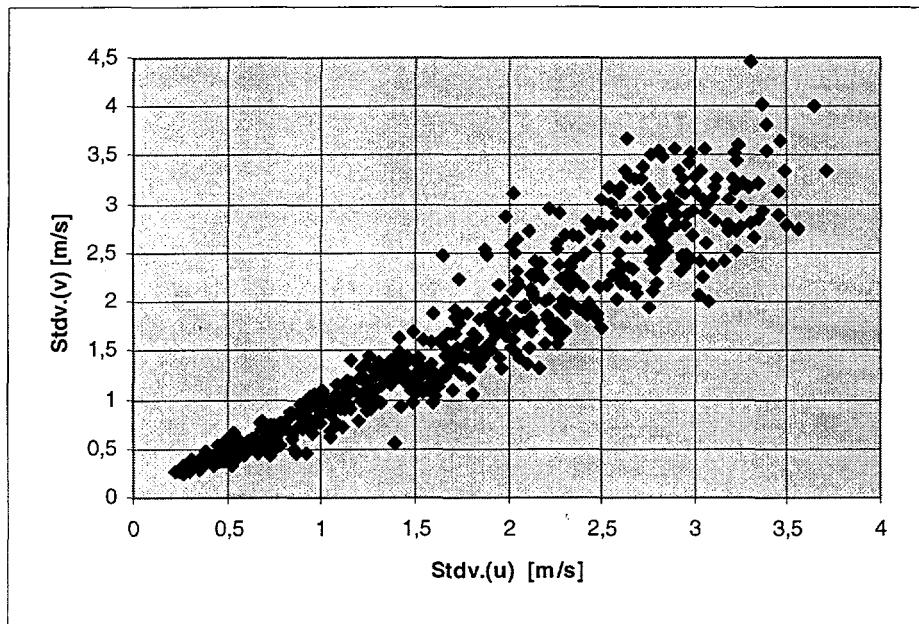


Figure 3.1-6 Standard deviation of the v turbulence component as function of standard deviation of the u turbulence component at level 42.7 m.

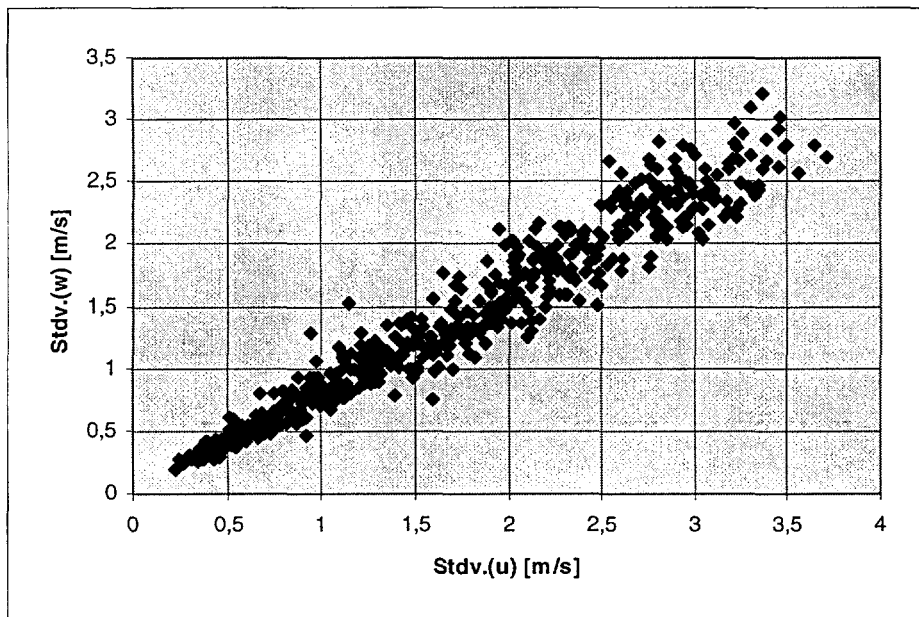


Figure 3.1-7 Standard deviation of the w turbulence component as function of standard deviation of the u turbulence component at level 42.7 m.

Compared to a flat terrain situation, the ratio between the standard deviations of the turbulence components are different in a complex mountainous terrain. In the Sky River case, the ratio between the v- and u-turbulence components is approximately 1.0, and the ratio between the standard deviations of the w- and the u-turbulence components is approximately 0.8.

In general the turbulence field in a complex mountainous terrain tends to be more isotropic compared to a flat terrain situation. This is also suggested in the above investigation of the turbulence intensities, and it is moreover reflected in length scales of the turbulence

components. For the Sky River site, the u-turbulence (Kaimal) length scale was found to be in the interval 600-800m, the v-turbulence (Kaimal) length scale in the interval 250-500m, and the w-turbulence (Kaimal) length scale in the interval 150-250m (Thomsen, 1996). The coherence decay constants, associated with the uu-, the vv-, and the ww-coherences, were determined to approximately 12, 7, and 5, respectively (Thomsen, 1996).

3.2 Load cases

Two different measured 10 minutes load cases are selected representing different mean wind speed and turbulence intensity regimes. The test cases are partly characterised by the parameters in Table 3.2-1.

	Load case 1	Load case 2
Mean wind speed (m/s)	11.6	20.5
Yaw error (deg.)	-10.0	-4.1
Turbulence intensity (%)	9.7	15.2

Table 3.2-1 Measured load cases.

The wind field modelling associated with the simulations are not able to take into account varying mean wind direction with height above terrain. Consequently, a compromise between the mean wind slope observed at levels 19.3m and 42.7m must be found. Based on the available information in Figure 3-1.1 and Figure 3-1.2, a representative mean wind slope equal to 8 deg. was selected for the present calculations.

An other important feature of the deterministic wind field is the mean wind shear, where a speed up effect at the position of the investigated turbine was observed. Based on an azimuthal binning of the flap root moment, performed for a number of measurements, the modelled mean wind shear was adjusted to obtain agreement between the averaged measured bin values and corresponding values, originating from simulations carried out neglecting the turbulent part of the external loading (Thomsen, 1996). The resulting shear field for load case 1 (including the effects from tower shadow) is presented if Figure 3.2-1.

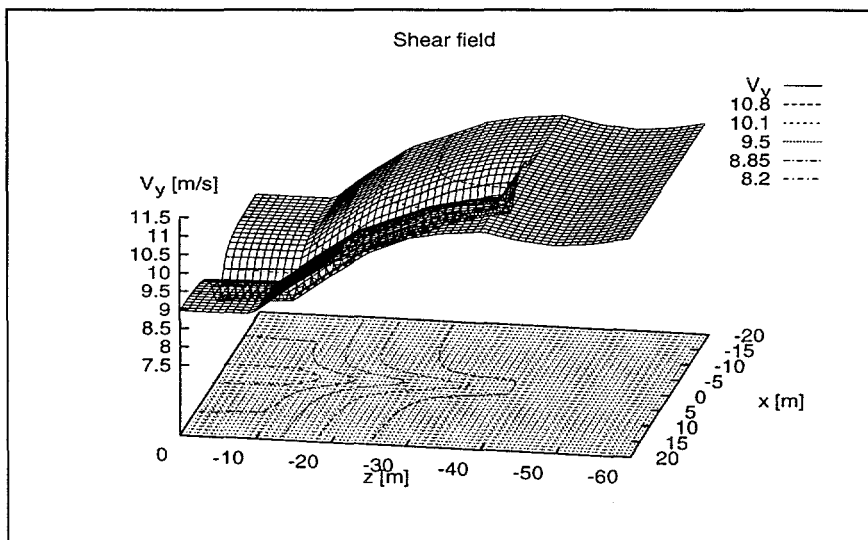


Figure 3.2-1 Resulting shear field for load case 1.

The turbulence field is based on the Mann model with a subsequent re-scaling of the individual turbulence components to obtain the required ratios between standard deviations of the turbulence components extracted in the previous section. Adjusting to measured power spectra of the u-turbulence component, a Mann turbulence length scale equal to 25m was selected.

4. Results

The validation is performed for the two load cases defined in the previous chapter. It is based on a comparison of measured and predicted flap and edge root moments as well as on the three (rotating) shaft moments. The comparison is carried out on a statistical basis as well as on power spectra level.

4.1 Statistics of measurements and predictions

The statistics in terms of average values, maximum values, minimum values, and standard deviations, for each of the selected structural loads, are presented in the figures and tables below. The statistics are based on 10-minute time series sampled with 32 Hz and covers a huge amount of measurements at different load conditions.

The results related to the flap wise loading are presented in Table 4.1-1, in Figures 4.1-1 and in Figure 4.1-2.

	Mean (kNm)	Max. (kNm)	Min. (kNm)	Stdv. (kNm)
Load case 1	170.0	249.6	97.1	19.5
Load case 2	113.0	328.4	-94.2	51.3

Table 4.1-1 Statistics of flap wise root moments from simulated results.

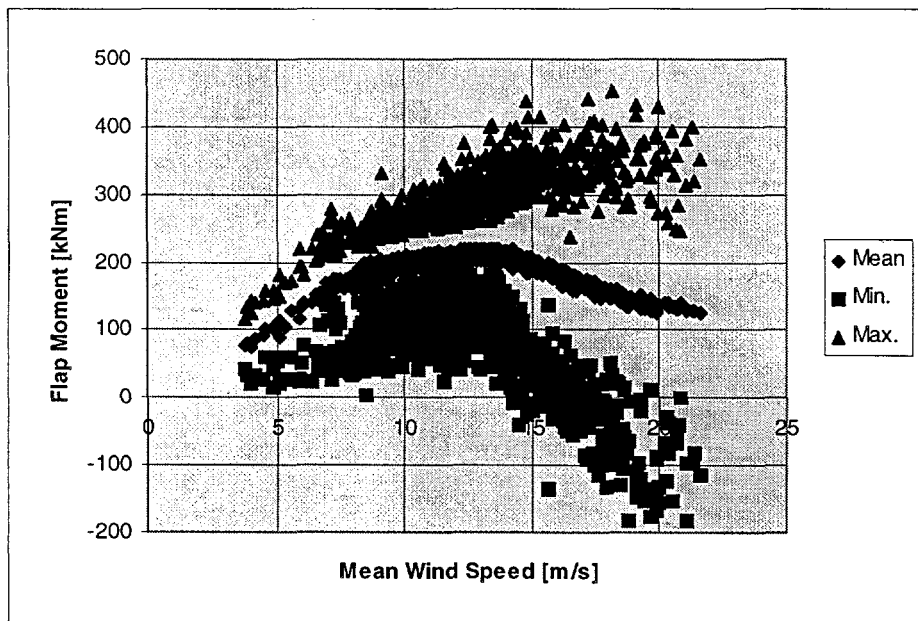


Figure 4.1-1 Mean, max., and min. of measured flap wise root moments as function of mean wind speed.

Comparing the predicted values in Table 4.1-1 with the measured values in Figure 4.1-1 and Figure 4.1-2, it is seen that the two test cases are in good agreement with the available measurements. There is a slight tendency of under predicting the mean values which probably can be attributed to drift of the strain-gauges.

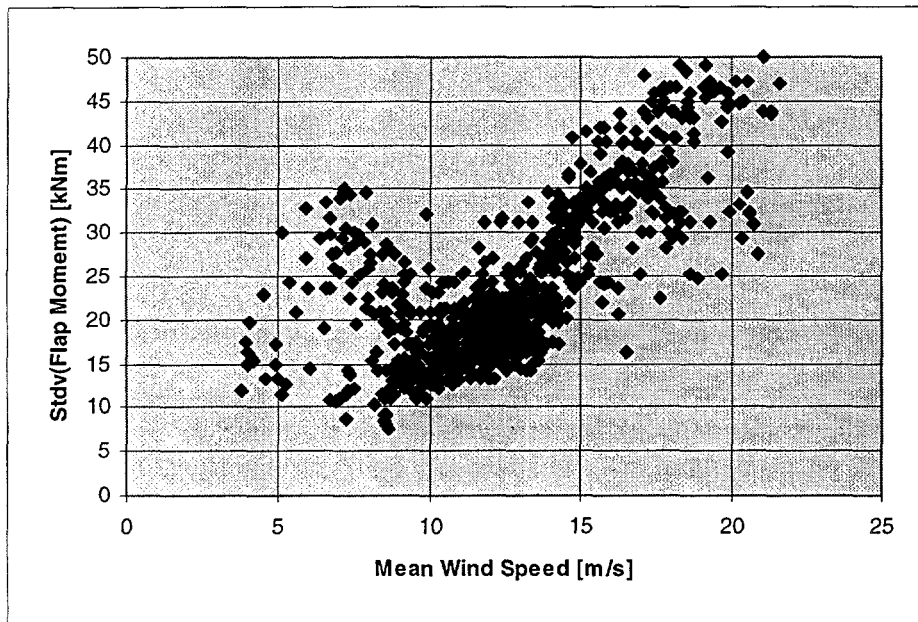


Figure 4.1-2 Standard deviation of measured flap wise root moments as function of mean wind speed.

The results for the edge wise root moments are presented in Table 4.1-2, in Figure 4.1-3, and in Figure 4.1-4. The standard deviation is primarily due to the gravitational loading and is consequently, as expected, not essentially influenced by the mean wind speed.

	Mean (kNm)	Max. (kNm)	Min. (kNm)	Stdv. (kNm)
Load case 1	30.0	114.4	-57.7	43.0
Load case 2	17.8	163.1	-113.1	43.4

Table 4.1-2 Statistics of edge wise root moments from simulated results.

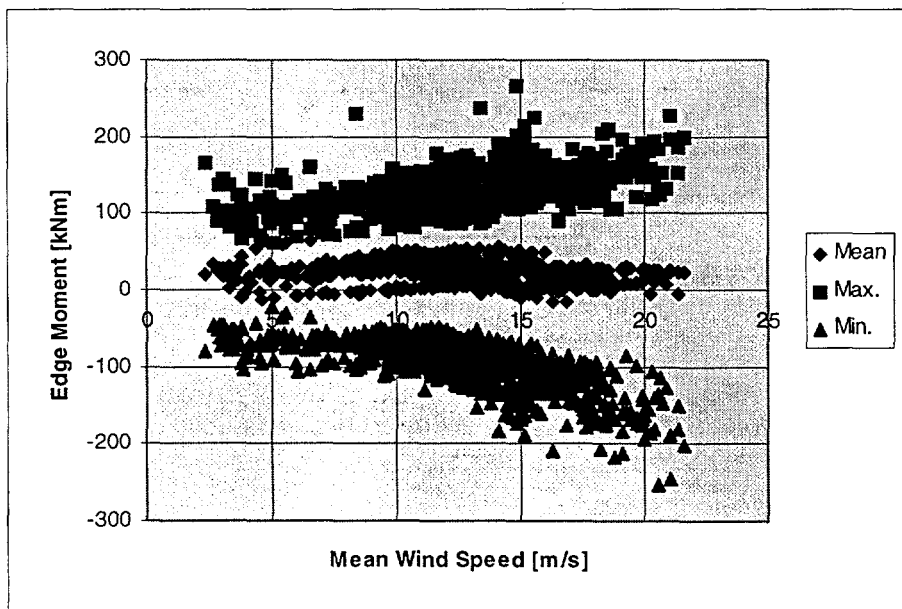


Figure 4.1-3 Mean, max., and min. of measured edge wise root moments as function of mean wind speed.

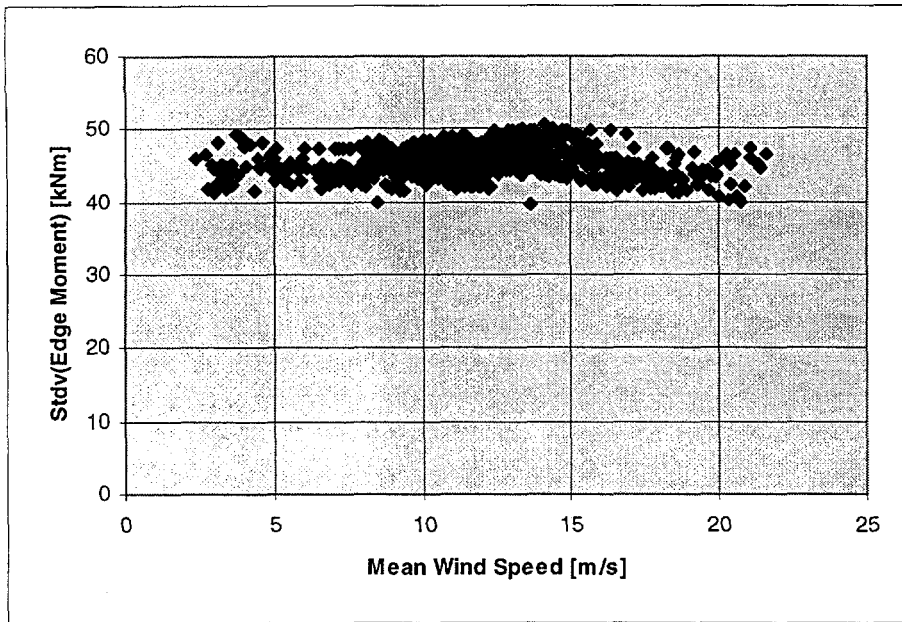


Figure 4.1-4 Standard deviation of measured edge wise root moments as function of mean wind speed.

For the edge wise root moment there is a slight tendency that the simulation underestimate the dynamics expressed by the standard deviation and the extreme values. Moreover, the mean values of the test cases differ (considerably) from the measured values, which is probably caused by drift in the strain gauges.

	Mean (kNm)	Max. (kNm)	Min. (kNm)	Stdv. (kNm)
Load case 1	-0.0	137.0	-131.2	43.6
Load case 2	-0.6	277.0	-235.4	65.9

Table 4.1-3 Statistics of shaft bending moments (M_x) from simulated results.

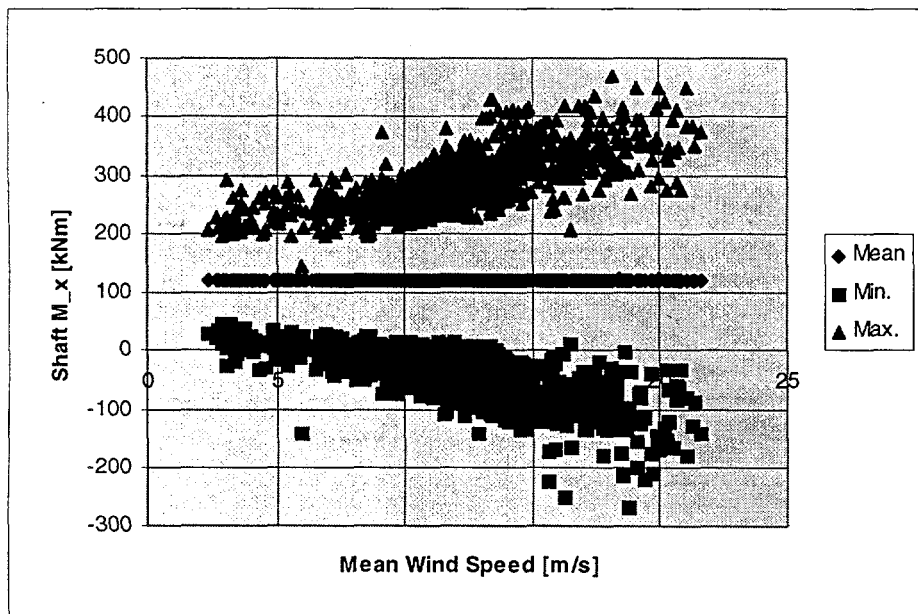


Figure 4.1-5 Mean, max., and min. of measured shaft bending moments (M_x) as function of mean wind speed.

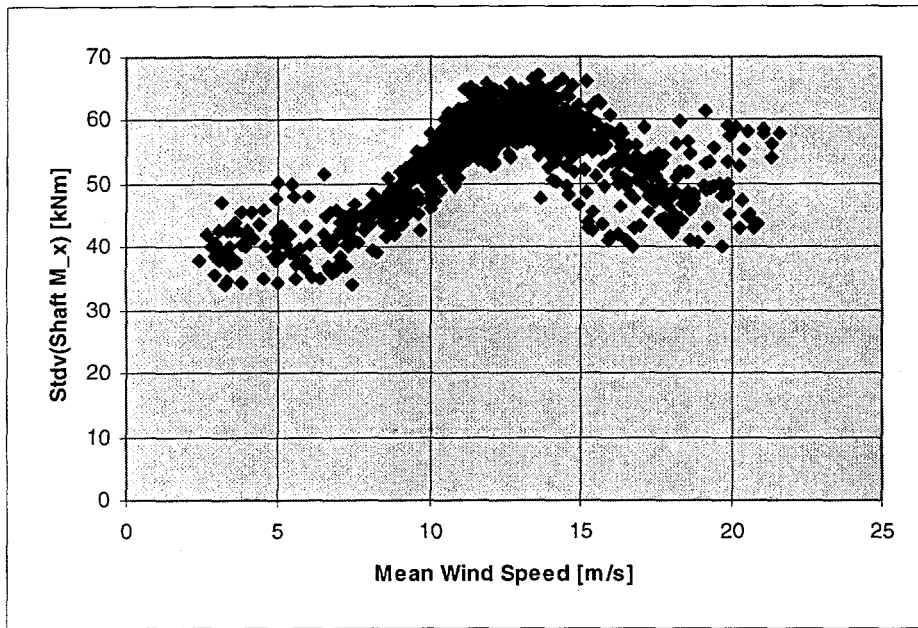


Figure 4.1-6 Standard deviation of measured shaft bending (M_x) moments as function of mean wind speed.

	Mean (kNm)	Max. (kNm)	Min. (kNm)	Stdv. (kNm)
Load case 1	-0.0	154.1	-114.4	43.5
Load case 2	-0.4	245.9	-236.9	64.9

Table 4.1-4 Statistics of shaft bending moments (M_y) from simulated results.

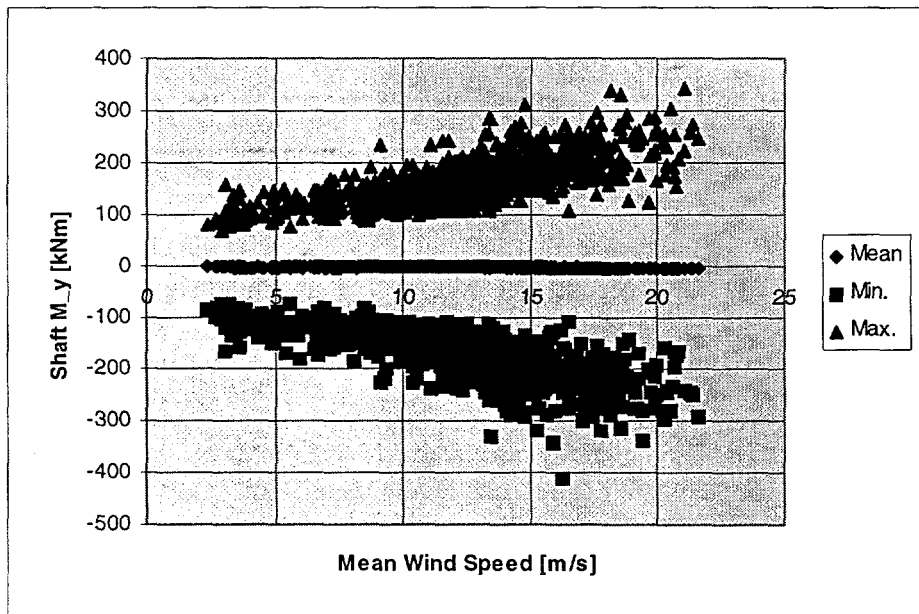


Figure 4.1-7 Mean, max., and min. of measured shaft bending moments (M_y) as function of mean wind speed.

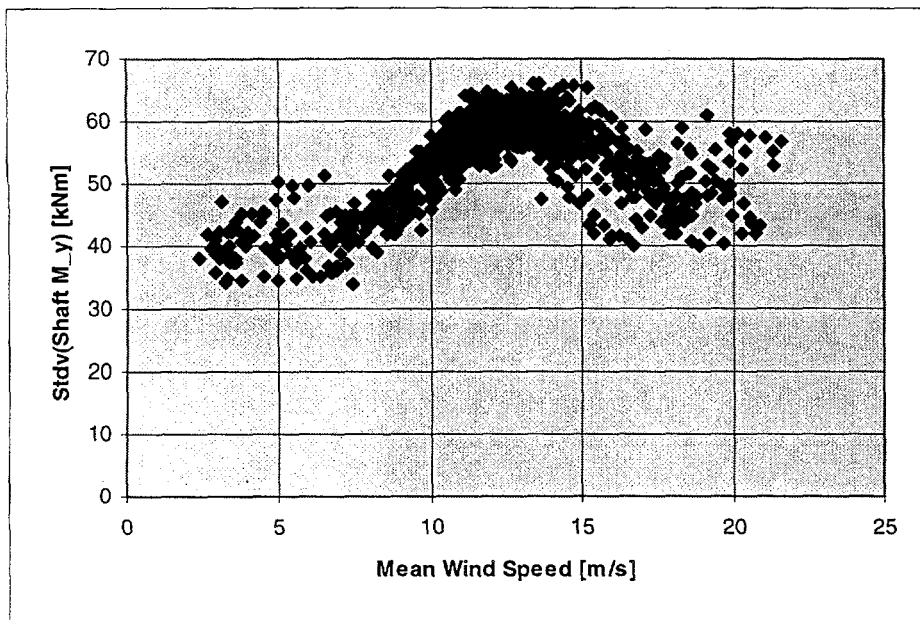


Figure 4.1-8 Standard deviation of measured shaft bending (M_y) moments as function of mean wind speed.

For measurements as well as for simulations it is observed that the statistics of the two shaft bending moments (denoted in the tables and figures by M_x and M_y , respectively), as expected, are much alike. The mean values and the standard deviations are almost identical, whereas slight deviations are observed for the extreme values. The deviation for the extreme values might be explained by the relatively less significant statistics of extremes in general, and the circumstance that, in the present situation, the extreme values are the result of a superposition of a periodic deterministic signal and a stochastic process. As the periodic deterministic components of the two shaft bending moments are not in phase, a possible large wind gust will result in different total response for the two shaft bending moments.

Comparing measurements with simulations, the mean values are identical and close to zero as would be expected. Concerning the standard deviation, the simulations are seen to underestimate somewhat for the medium wind speed load case and overestimate slightly for the high wind speed load case. The extremes are of the same order of magnitude for simulations and for measurements.

The statistics of the simulated shaft torsion moments are presented in Table 4.1-5. The statistics of the measured shaft torsion moments are shown in Figure 4.1-9 and in Figure 4.1-10, respectively.

	Mean (kNm)	Max. (kNm)	Min. (kNm)	Stdv. (kNm)
Load case 1	104.3	136.9	62.8	12.3
Load case 2	171.1	313.9	49.4	36.2

Table 4.1-5 Statistics of shaft torsion moments from simulated results.

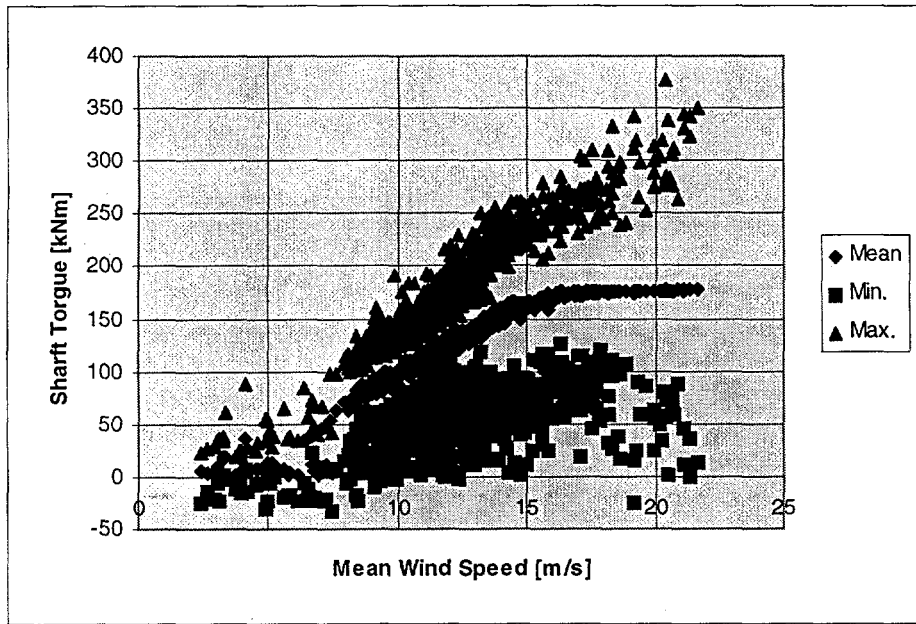


Figure 4.1-9 Mean, max., and min. of measured shaft torsion moments as function of mean wind speed.

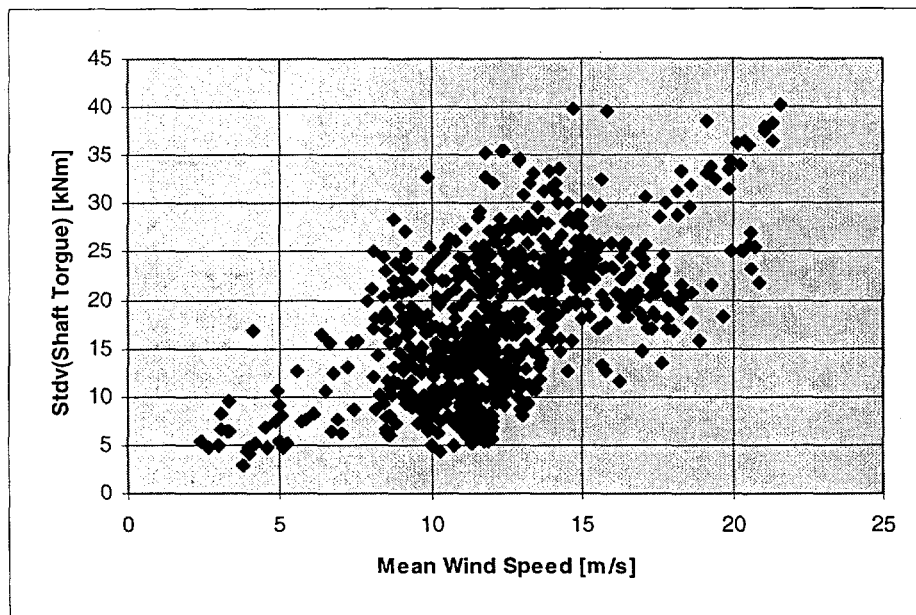


Figure 4.1-10 Standard deviation of measured shaft torsion moments as function of mean wind speed.

The measured mean values in Figure 4.1-9 reflects the expected power curve shape. Comparing simulated results with measured results, it is seen that both the static part of the signal, represented by the mean value, and the dynamic part, represented by the standard deviation and the extreme values, are in excellent agreement.

In conclusion, it is demonstrated that, for the investigated load cases, the simulated statistics are in satisfactory agreement with measured statistics. For the blade loads, the observed deviations between measured and predicted mean values are caused by drift of the

measurements due the fact that these signals, in contradiction the shaft measurements, are based in strain gauges mounted on GRP (glass fibre polyester).

4.2 Power spectra of measurements and predictions

The present section deals with a comparative analysis of power spectra of measured and simulated results originating from identical load conditions (load case 1 and load case 2 defined in section 3.2). The presented power spectra are based on 10-minute time series sampled with 32 Hz and have been averaged using 16 segments.

The spectra of the along wind turbulence component are shown in Figure 4.2-1 and in Figure 4.2-2 for the two load cases. The spectra refer to hub height. The along wind turbulence component is the main responsible for the stochastic loading of the turbine, and a satisfactory agreement between the simulated and the measured turbulence is seen.

The results for the flap wise root bending moments are presented in Figure 4.2-3 and Figure 4.2-4. As expected, the power spectra contains peaks on multiples of 1P (originating from the rotating wind turbulence) and on the blade flap wise natural frequency of 1.68 Hz. The general agreement between measurements and simulations is good both for load case 1 and for load case 2, although there is a tendency that the prediction somewhat overestimates the peaks at 2P and 3P in the load case 1 situation, and further overestimate the peak at 3P in the case of the high wind situation (load case 2). However, the deviations are moderate and might be explained by deviations in the measured and the generated rotating wind spectrum.

The results from the edge wise blade root moments are illustrated on the Figures 4.2-5 and 4.2-6. An excellent agreement between measured and simulated results is observed both concerning the spectral peaks on multiples of 1P and the peak representing the first blade edge wise natural frequency of 2.75 Hz. The peak at 1P is the overall dominating and contains contribution from turbulence and in particular from gravity.

The results from the shaft bending moments are presented in Figure 4.2-7 and in Figure 4.2-8. As seen, these power spectra, in general, display a very satisfactory agreement between measurements and simulations. The spectra contains peaks at multiples of 1P originating from the rotating turbulence spectrum, superimposed at 1P by a deterministic contribution from the gravity and at 3P by a deterministic contribution from mean wind shear, tilt, yaw error, and tower shadow.

The power spectra of the shaft torque are shown in Figure 4.2-9 and in Figure 4.2-10. In general, a satisfactory agreement between predictions and measurements is recorded. For an ideally balanced rotor, spectral peaks only at multiples of 3P should be expected. However, the measured results, in addition to that, display a peak at 1P for load case 1, which possibly reflects a (weak) rotor asymmetry, although it is not found in the spectrum associated with load case 2. Finally, there is a tendency that the measured peaks are broader than the simulated.

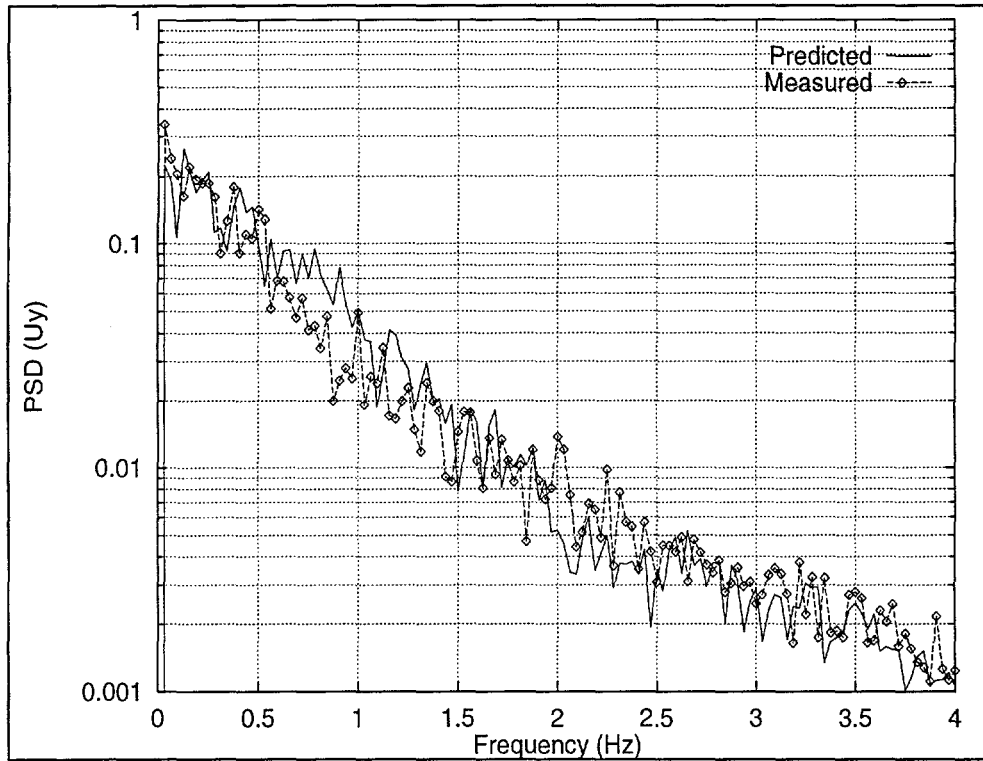


Figure 4.2-1 Measured and predicted power spectrum of the longitudinal turbulence component (Uy) related to load case 1.

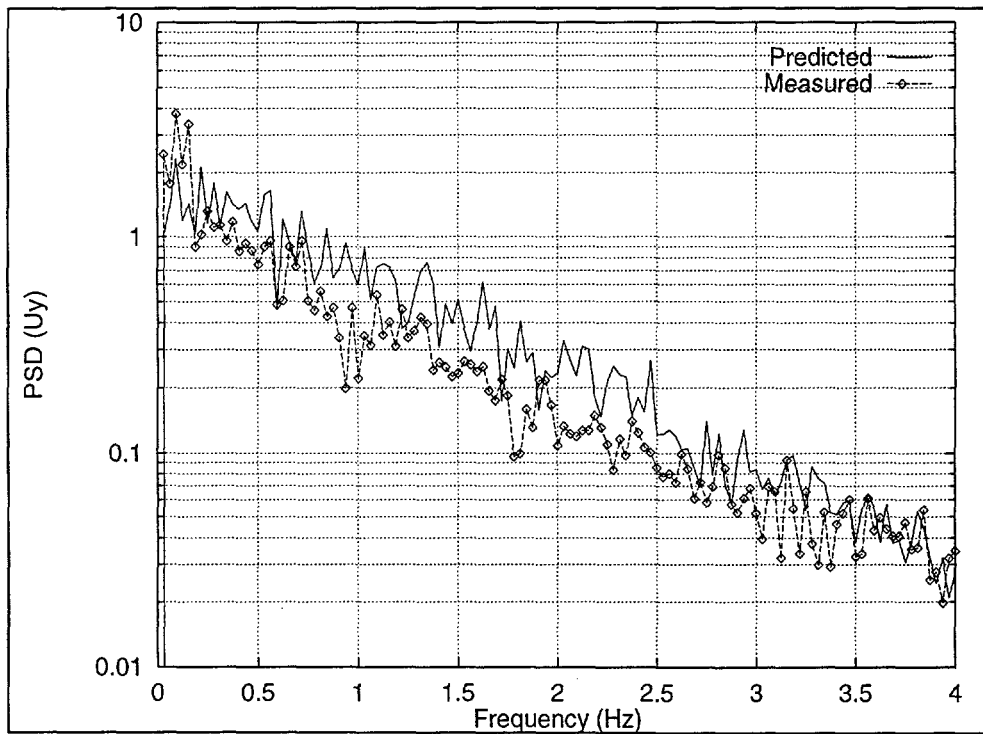


Figure 4.2-2 Measured and predicted power spectrum of the longitudinal turbulence component (Uy) related to load case 2.

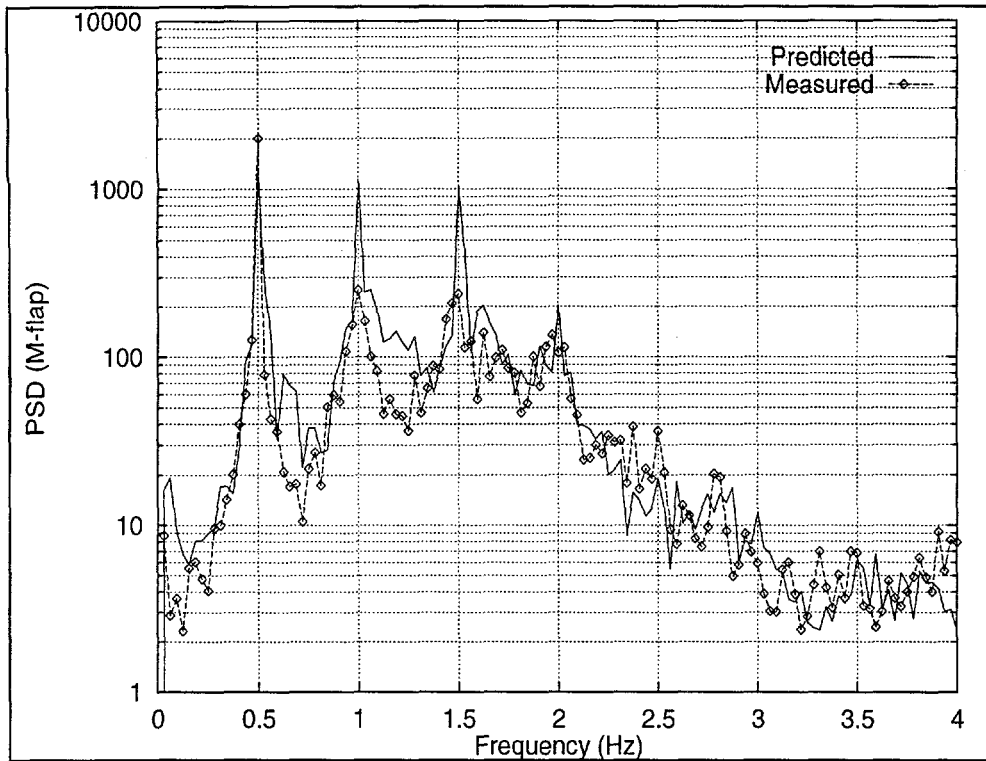


Figure 4.2-1 Measured and predicted power spectrum of flap wise blade root moment related to load case 1.

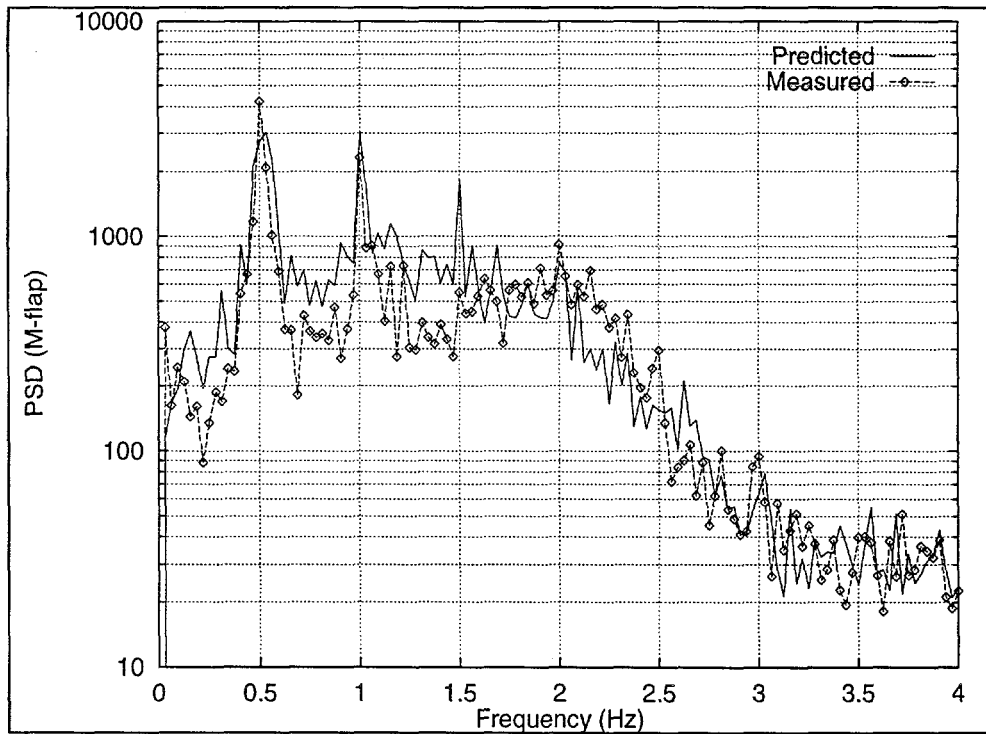


Figure 4.2-2 Measured and predicted power spectrum of flap wise blade root moment related to load case 2.

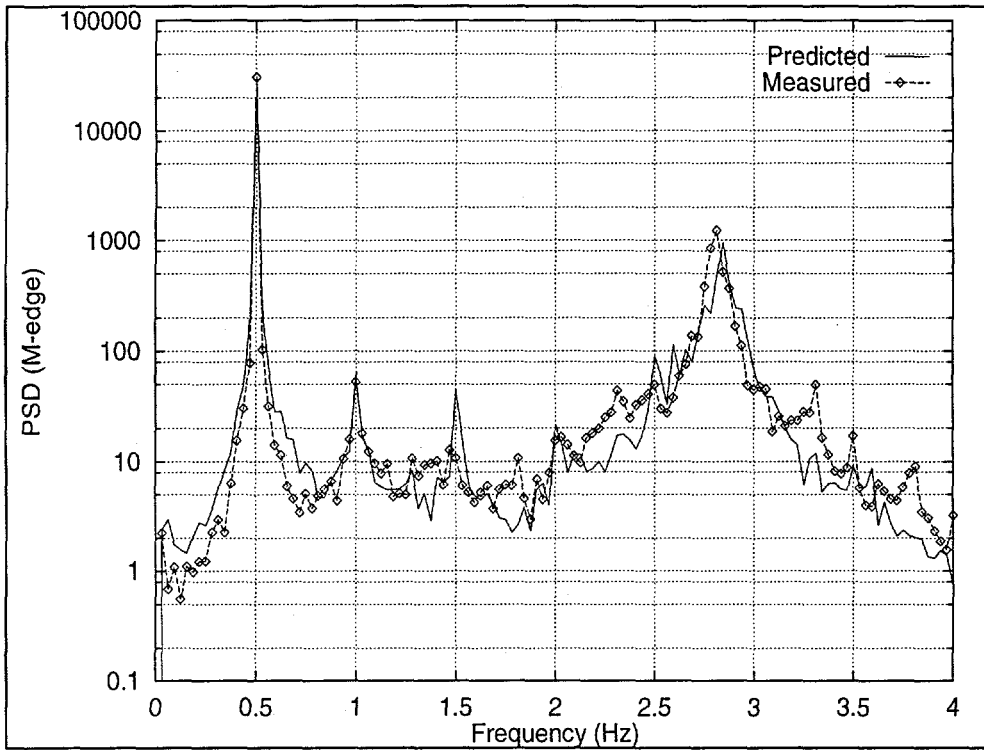


Figure 4.2-3 Measured and predicted power spectrum of edge wise blade root moment related to load case 1.

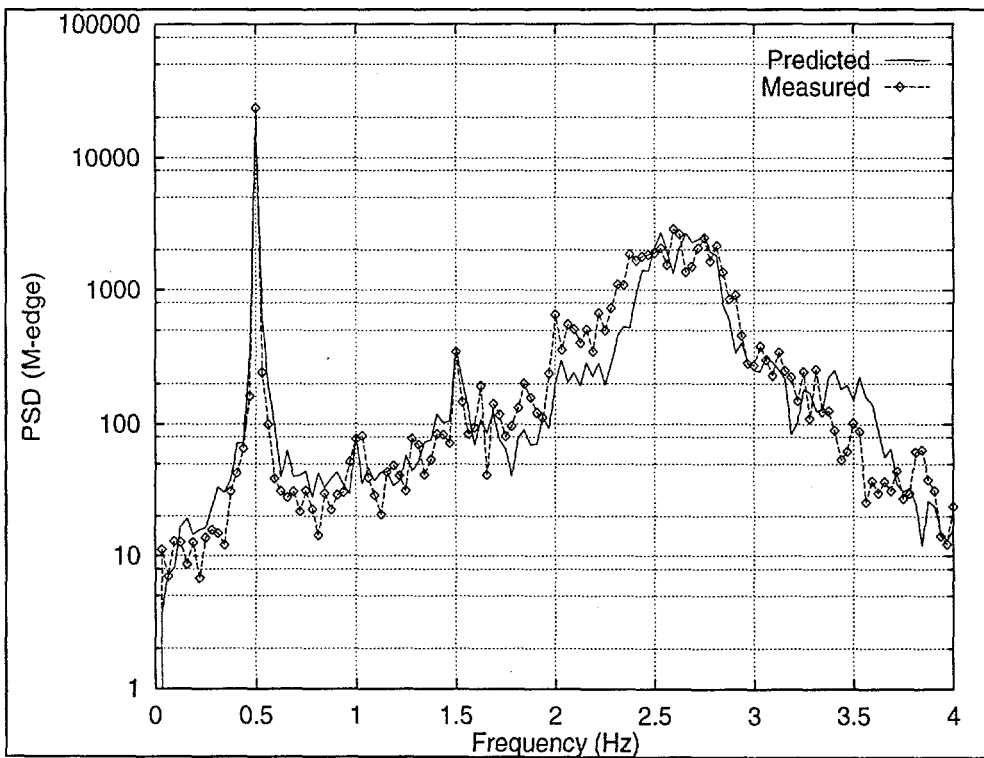


Figure 4.2-4 Measured and predicted power spectrum of edge wise blade root moment related to load case 2.

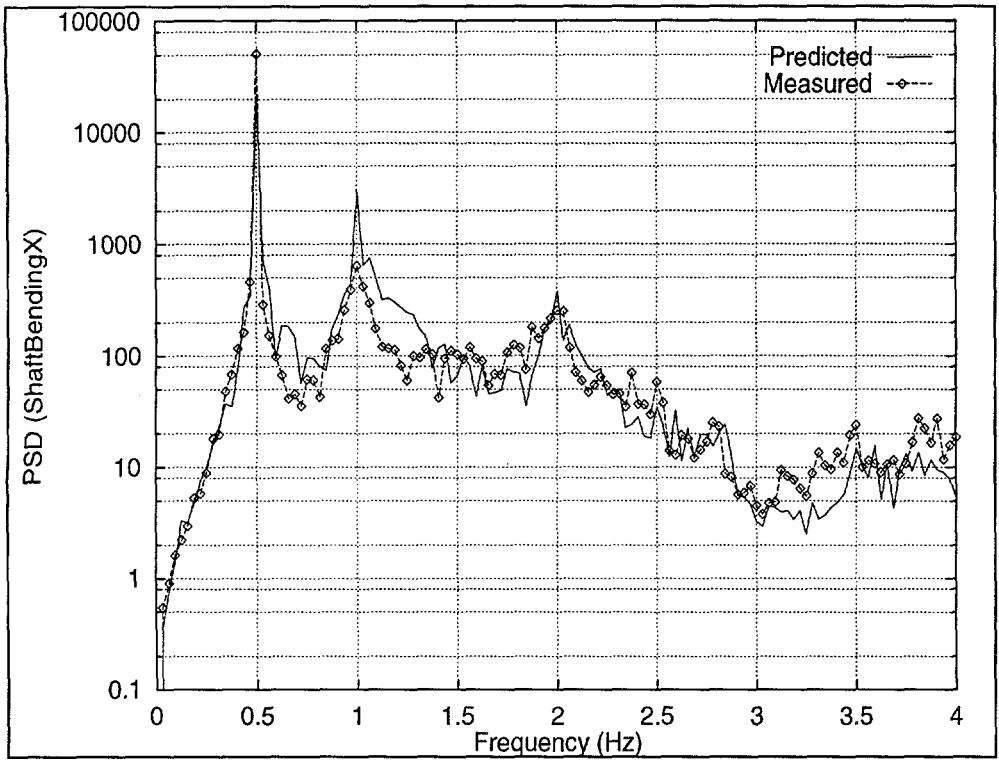


Figure 4.2-5 Measured and predicted power spectrum of shaft bending moment related to load case 1.

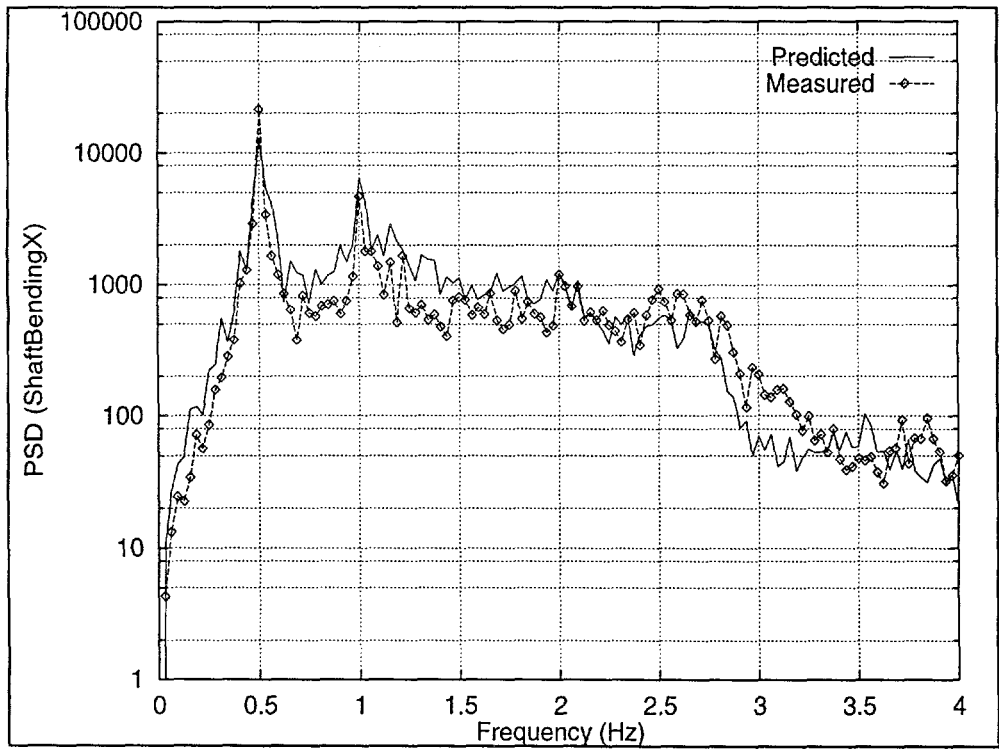


Figure 4.2-6 Measured and predicted power spectrum of shaft bending moment related to load case 2.

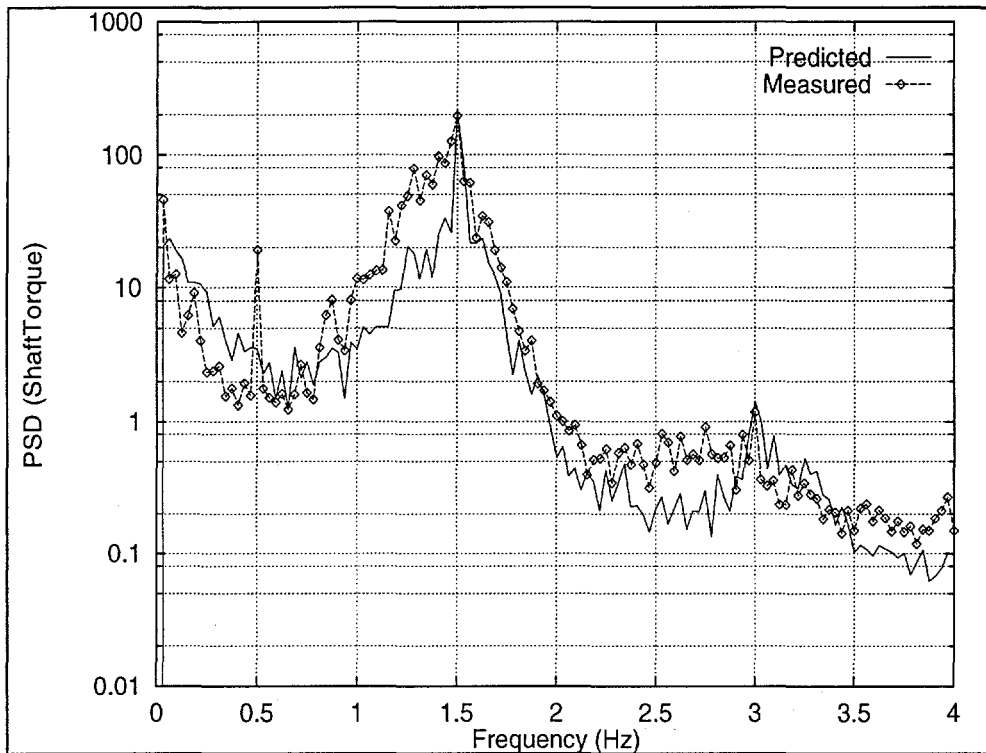


Figure 4.2-7 Measured and predicted power spectrum of shaft torsion moment related to load case 1.

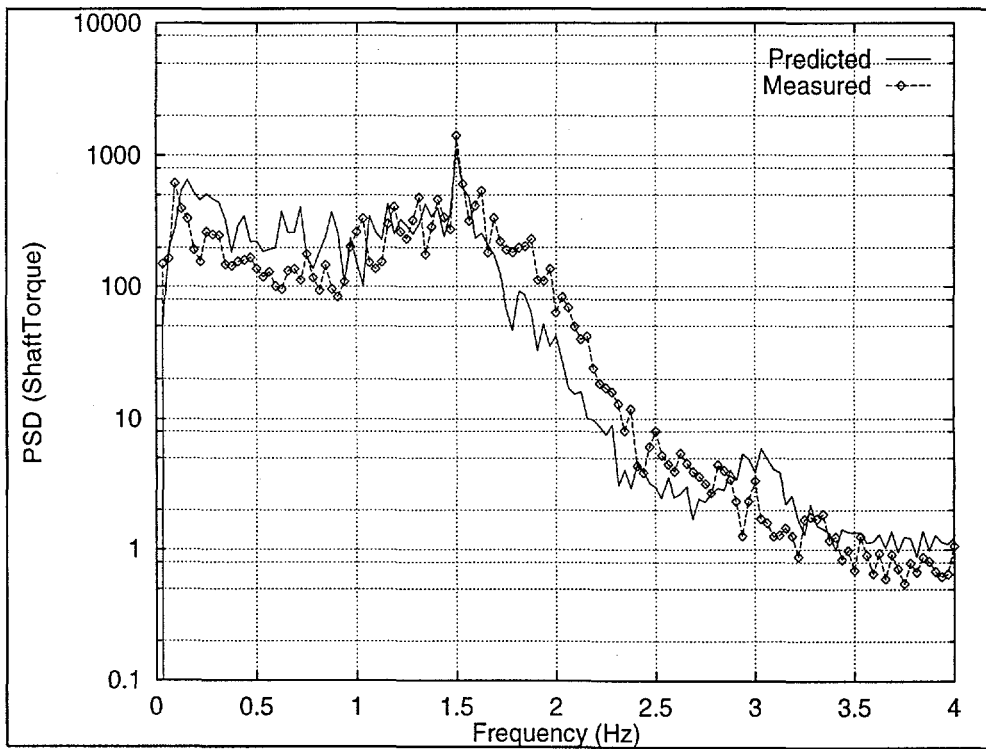


Figure 4.2-8 Measured and predicted power spectrum of shaft torsion moment related to load case 2.

5. Conclusion

In conclusion, the comparison of measurements and predictions shows that the present model is fully acceptable compared to state of the art in aeroelastic wind turbine modelling.

It is demonstrated that, for the investigated load cases, the simulated statistics are in satisfactory agreement with the measured statistics. For the blade loads, some deviations between measured and predicted mean values are observed which are likely to be caused by drift of the measurements as these particular signals, in contradiction the shaft measurements, are based in strain gauges mounted on glass fibre.

The detailed character of the dynamics of the wind loading and of the structural system are investigated by comparing measured and simulated power spectra of selected loads. The outcome of this part of the analysis is a convincing agreement both with respect to energy content on the different multiples of 1P and on the relevant natural frequencies. For the shaft torsion moment a small unbalance of the measured loads is recorded. This is, however, of very modest magnitude, and it was consequently not found worthwhile to attempt to capture that in the simulations.

6. References

- Mann, J. (1994). Models in Micrometeorology. Risø-R-727(EN). Risø National Laboratory, Roskilde, Denmark.
- Petersen, S.M (1994). Wind Turbine Test. VESTAS V39 - 500 kW. System Test. Risø-I-807 (EN). Risø National Laboratory, Roskilde, Denmark.
- Thirstrup Petersen, J. (1990). Kinematically Nonlinear Finite Element Model of a Horizontal Axis Wind Turbine. Part 1 and 2. Risø National Laboratory, Roskilde, Denmark.
- Petersen, S.M., Thomsen, K., Paulsen, U.S, and Pedersen, T.F. (1994). Load Measurements on a pitch Regulated Wind Turbine in Inhomogeneous Terrain at Sky River - Vestas V39. Risø-I-834 (EN). Risø National Laboratory, Roskilde, Denmark.
- Thomsen, K., Petersen, S.M., Petersen, J.T., Øje, S., and Friedrich, M. (1996). Terrain Induced Loads on Pitch Regulated Wind Turbines. Risø-R-846 (EN). Risø National Laboratory, Roskilde, Denmark.

Title and authors

Validation of an Aeroelastic Model of Vestas V39

Gunner Chr. Larsen and Per Vølund

ISBN

87-550-2391-6

ISSN

0106-2840

Department or group

Wind Energy and Atmospheric Physics Department

Date

April 1998

Groups own reg. number(s)

1120058-00

Project/contract No(s)

JOR3-CT95-0033

Pages

30

Tables

6

Illustrations

31

References

5

Abstract (max. 2000 characters)

An aeroelastic model of the pitch controlled Vestas V39 wind turbine is validated by comparing simulations with measurements. The comparison is carried out on a statistical basis as well as on a power spectra level, and the model is found to be good compared to state of the art aeroelastic wind turbine modelling.

The aeroelastic code used is HawC, which has been developed at Risø, and the turbulence model is the Mann model. The measurements used for validation were carried out in a complex mountainous terrain at Sky River in California.

The model is developed with the purpose of investigating load sensitivity to wind and turbulence parameters, for a complex terrain, in the project COMTERID.

Descriptors INIS/EDB

AERODYNAMICS; COMPUTERIZED SIMULATION; ELASTICITY; EXPERIMENTAL DATA; HORIZONTAL AXIS TURBINES; TURBULENCE; WIND LOADS.

Available on request from Information Service Department, Risø National Laboratory, (Afdelingen for Informationsservice, Forskningscenter Risø), P.O.Box 49, DK-4000 Roskilde, Denmark. Telephone +45 46 77 40 04, Telefax +45 46 77 40 13